Faraday Discussions

Cite this: *Faraday Discuss.*, 2017, **196**, 219

PAPER

View Article Online
View Journal | View Issue

Construction and function of a highly efficient supramolecular luminescent system†

Yingjie Liu, Suqian Ma, Bin Xu* and Wenjing Tian*

Received 3rd July 2016, Accepted 9th August 2016

DOI: 10.1039/c6fd00166a

Aggregation-induced emission (AIE) provides a new way of achieving highly efficient luminescent materials. In this contribution, the self-assembly behavior, molecular stacking structure and photophysical properties of two polymorphs of a supramolecular co-crystal (C1 and C2) are investigated. The block-like crystal C1, packed in segregated stacking with strong π–π interactions between the **H** and **G** molecules, shows weak green emission with a low efficiency (Φ_F) of 2%. In comparison, the needle-like crystal C2, packed in segregated stacking with no obviously strong intermolecular interactions, shows bright yellow emission. More importantly, C1 exhibits mechanochromic behavior.

Introduction

Organic luminescent materials have attracted intense interest over the past decade due to their wide potential applications in the optoelectronic and biological fields.[1–4] The optical properties of organic materials in practical applications, which essentially deal with the aggregate state, are defined not only by the chemical structure of the luminescent molecules themselves but also by the nature of their intermolecular electronic coupling.[5] Once an organic luminescent molecule is excited by the absorption of a photon, it can return to the ground state with the emission of fluorescence, but many other pathways for de-excitation are also possible: internal conversion, intersystem crossing, intramolecular charge transfer, conformational change, *etc.* Interactions in the excited state between molecules, especially neighbouring molecules in the aggregate state, such as electron transfer, proton transfer, energy transfer, and excimer or exciplex formation, may also compete with de-excitation. The features of these interactions in the aggregate state are usually affected by the relative orientation of the neighbouring molecules, which is induced through supramolecular interactions

---

State Key Laboratory of Supramolecular Structure and Materials, Jilin University, Qianjin Street No. 2699, Changchun 130012, China. E-mail: xubin@jlu.edu.cn; wjtian@jlu.edu.cn

† Electronic supplementary information (ESI) available. CCDC 1486884 and 1486885. For ESI and crystallographic data in CIF or other electronic format see DOI: 10.1039/c6fd00166a

between the molecules during the aggregate formation process. The fluorescence characteristics, such as the spectrum, quantum yield and lifetime, will thus be affected by any excited state process involving interactions of the excited molecule with its close environment. For this reason, most organic fluorescent materials have strong emission and a high quantum yield in solution, but the quantum yield generally drops in the solid state. This aggregation caused quenching (ACQ) effect has limited the scope of the technological applications of organic luminescent materials.[6,7]

The discovery of aggregation-induced emission (AIE) or aggregation-enhanced emission (AEE) provides a new way to solve aggregation quenching and offers opportunities to develop useful luminescent materials.[8] The AIE luminophors are non-emission in the isolated state but highly emissive in the aggregate state, whereby active intramolecular motions including rotation and vibration can effectively dissipate the exciton energy and the restriction of intramolecular motion (RIM) can boost radiative transition, respectively. Attracted by the fascinating features of AIE, a large variety of AIE molecules have been developed with great structural diversity.[9–11] Moreover, the applications of AIE molecules have given rise to new developments in an array of fields, ranging from fundamental optoelectronics,[12–14] sensing,[15–18] and bioimaging[19–21] to complicated stimuli-responsive systems.[22–26] However, aggregation structures with various supramolecular interactions including π–π interactions, H-bonds and dipole–dipole interactions are difficult to manipulate. Thus, a major challenge that needs to be addressed is how to construct highly efficient luminescent systems with the desired chemical and physical properties by controlling the molecular stacking modes and the consequent intermolecular interactions.

Aiming to address this issue, we suppose that manipulating the stacking modes of AIE luminogens through supramolecular self-assembly may provide a new potential solution to developing highly efficient luminescent supramolecular systems and exploring the new functions of AIE molecules.[27] In contrast to the traditional luminescent materials as host molecules, the AIE-active materials will provide more variety in molecular stacking mode since the molecules possess a twist conformation and exhibit weak intermolecular interactions in the solid state. In this respect, it is essential to establish a molecular level understanding of the correlations between the molecular structure, stacking modes, and photophysical properties.

The crystalline state of molecules offers a well-defined platform to investigate the supramolecular interactions in the aggregate state,[28–30] since it can be described as a supramolecular network where reliable and accurate information on the relative orientation and nature of the intermolecular interactions of the adjacent molecules can be obtained through crystallography. Herein, we demonstrate that the optical properties of a supramolecular luminescent system with an AEE-active molecule (BP4VA) serving as the luminescent host (**H**) and an aromatic molecule (FIB) as the guest (**G**) (see Scheme 1) in the crystalline state can be tuned using the co-crystal strategy through supramolecular self-assembly. Two polymorphs of the co-crystal can be easily obtained by slow solvent evaporation at room temperature under the rigorous exclusion of light. A structural and spectroscopic study allows us to understand the relevant structure–property relationships in this unique class of luminescent co-crystal materials. Furthermore, we explore their application in solid state stimuli response luminescence.

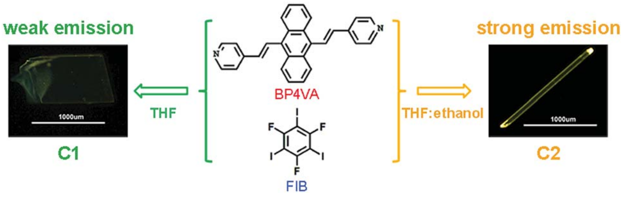

Scheme 1 Schematic illustration of the co-crystal system and chemical structures of BP4VA and FIB.

Experimental

Materials

All materials were purchased from either Acros or Aldrich Chemical Co. and used without further purification. THF was dried by distillation from sodium/benzophenone under nitrogen.

Instrumentation

^{1}H NMR spectra were recorded using a Bruker AVANCE 500 MHz spectrometer with tetramethylsilane as the internal standard. Time of flight mass spectra were recorded using a Kratos MALDI-TOF mass system. UV-vis absorption spectra were recorded using a Shimadzu UV-3100 spectrophotometer. Photoluminescence spectra were collected using a Maya 2000Pro. optical fiber spectrophotometer. Crystalline state PL efficiencies were measured with an integrating sphere (C-701, Labsphere Inc.) with a 365 nm Ocean Optics LLS-LED as the excitation source, and the laser was introduced into the sphere through optical fiber. Fluorescence microscopy images were obtained using an Olympus BX51 fluorescence microscope.

Preparation of samples and emission spectra measurement

Co-crystals C1 and C2 were prepared by slow solvent evaporation at room temperature under the rigorous exclusion of light. In a typical experiment, BP4VA and FIB were mixed in a molar ratio of 1 : 1 and dissolved in THF solution for C1, while for C2, BP4VA and FIB were dissolved in THF and ethanol mixed solvent. The emission spectra of the crystals were recorded according to the following procedure. The large-scale crystal samples were stuck on the surface of the substrate by non-emissive silica grease, and placed in the optical path of the exciting light source. A quartz cell was used to measure the solution emission spectra.

Morphology prediction

The growth morphologies of the co-crystal were calculated using the Materials Studio software, based on the attachment energy theory. The molecular structure was first optimized on the basis of the experimental crystal structure. The geometric and energy calculations were performed using the Forcite and Morphology modules.

X-ray crystallography

The diffraction experiments were carried out using a Rigaku R-AXIS RAPID diffractometer equipped with Mo KR and Control Software, using the RAPID AUTO at 293 K. Empirical absorption corrections were applied automatically. The structures were solved with direct methods and refined with a full-matrix least-squares technique, using the SHELXS v. 5.1 programs, respectively. The space groups were determined from the systematic absences and their correctness was confined by successful solution and refinement of structures. Anisotropic thermal parameters were refined for all the non-hydrogen atoms. The hydrogen atoms were added in idealized positions and refined with isotropic displacement. Crystallographic data and structure refinements for the structures reported in this paper are given in Table S3. CCDC 1486884–1486885 contain the supplementary crystallographic data for this paper.†

Results and discussion

BP4VA was synthesized using the procedure in our previous report[31] and FIB was purchased from Aldrich; their chemical structures are shown in Scheme 1. BP4VA is a derivative of DSA, a typical AIE luminogen. The introduction of pyridine units is expected to result in various different potential halogen or hydrogen bond interaction modes with the guest. In addition, the twist conformation of BP4VA allows more topological space in the aggregate state, although weakens the intermolecular interactions, which may be beneficial to the formation of co-crystals by interacting with the guest molecule. As a convenient method of controlling supramolecular interactions between BP4VA and FIB, two polymorphs of the co-crystal, named C1 and C2, were prepared by vaporizing mixed solvents with different ratios. X-ray analysis of the C1 and C2 co-crystals confirmed the 1 : 1 stoichiometry within a monoclinic system and space group $P2_1/c$ for C1, and a triclinic system and space group $P\bar{1}$ for C2. In the two polymorphs C1 and C2, BP4VA possesses one crystallographic conformation in the crystal, which is highly twisted in both, with dihedral angles of 66.09° and 54.32° between the central anthracene and double bond, respectively (Fig. 1 and 2). The twist conformation of BP4VA in the co-crystal was similar with that in its pure crystal state.[31] Notably, the molecules in C2 have a relatively smaller dihedral angle than those in C1 and the pure BP4VA crystal, suggesting extended conjugation along the long axis. Owing to the almost orthogonal conformation, there are almost no strong interactions in the pure BP4VA crystal, resulting in high efficiency luminescence.[32] Thus, we anticipate that the introduction of guest molecule FIB can not only tune the supramolecular interactions but also retain the highly emissive features.

C1 consists of segregated **H** and **G** molecular columns (see Fig. 1). In the **H** molecular column, the intermolecular **H**–**H** distance is 8.69 Å, which is much larger than the sum of the van der Waals' radii (3.4 Å) of carbon atoms, indicating the weak interactions between the luminescent host molecules. Interestingly, each **G** molecule forms two types of strong interaction with the adjacent two **H** molecules,[33] where the intermolecular **G**–**H** distances range from 3.65 Å to 3.70 Å (for detailed data see Table S1†). These unique interactions may form two types of local H-aggregate from one **G** molecule with the adjacent two **H** molecules, in which one is located between the pyridine unit of the adjacent **H** molecule and **G**

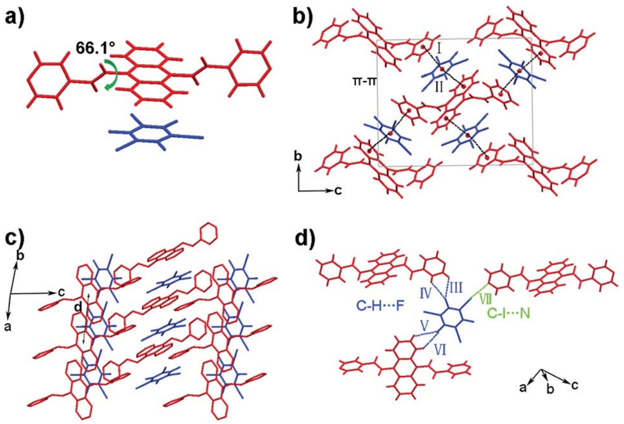

Fig. 1 (a) Conformational structures of BP4VA and FIB in the crystal. (b) Unit cell structure of C1 and the π–π interactions between the **H** and **G** columns. (c) Stacking of the molecular columns and (d) intermolecular interactions. BP4VA is drawn in red and FIB is drawn in blue. $d = 8.69$ Å.

molecule, and the other one is located between the peripheral benzene ring of the central anthracene in the opposite neighbouring **H** molecule and **G** molecule. These local H-aggregates will affect the photophysical process although there are no obvious strong intermolecular interactions between the adjacent **H** molecules. In addition, there also exist various C–H···F and C–I···N interactions among the adjacent **G** and **H** molecules.[34,35] These strong interactions and hydrogen or halogen bonds as the self-assembly driving forces along distinct directions make the molecules aggregate and expand into a layered structure, thus leading to a unique block-like crystal morphology.

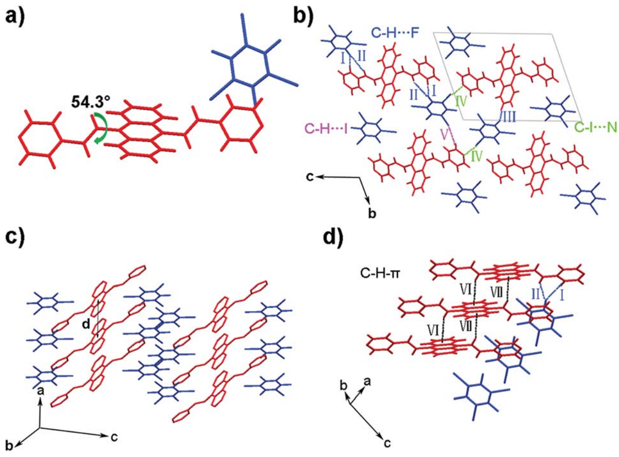

Fig. 2 (a) Conformational structures of BP4VA and FIB in the crystal. (b) Unit cell structure of C2 and the interactions between the **H** and **G** molecules. (c) Stacking of the molecular columns and (d) intermolecular interactions. BP4VA is drawn in red and FIB is drawn in blue. $d = 5.14$ Å.

The equilibrium morphology of C1, as predicted by Materials Studio software, shows a block-like crystal with its dominant (100) plane possessing an intersection angle of 78° as shown in Fig. 3a. Optical images (Fig. 3b) also confirm that the block-like C1 has an intersection angle of 78°, which is similar to that of the BP4VA crystal.

Similar to the C1 stacking mode, C2 also consists of segregated **H** and **G** molecular columns, and the **H** and **G** molecules keep the same orientation in each molecular column. In the **H** molecular column, the large distance (5.14 Å) between the central anthracenes of the adjacent molecules indicates that there is almost no face-to-face interaction and the **H** molecules adopt a stacking mode with J-aggregation. Instead, there are two different types of CH–π interaction between neighbouring molecules in the **H** molecular column. The interaction distance and the angle of the CH–π center for VI are 2.77 Å and 147.84°, and for VII are 2.78 Å and 147.84°, respectively. These CH–π interactions act as the driving force for close stacking along the *b* axis. Meanwhile, the **G** molecular columns are formed by relatively weak interactions, communicating with the adjacent **H** molecular column by three types of F···H interactions and one type of N···I halogen bond, as shown in Fig. 3 (detailed data is listed in Table S2†). These intermolecular interactions, stretching along distinct directions, are responsible for the resulting segregated-stacking modes. Morphology predictions indicate that C2 may grow along the [100] direction, and the lowest attachment energy for the (001) face suggests that it will be prominent in the crystal morphology. The needle-like C2 crystal can be confirmed by the optical image shown in Fig. 3.

As mentioned above, C1 and C2 are supramolecularly prepared by vaporizing the mixed solution, in which BP4VA and FIB recognize each other and self-assemble in an ordered way *via* non-covalent supramolecular interactions. Through controlling the growth environment, the BP4VA and FIB molecules not only assemble into a block-like morphology, but also form the needle-like micrometer crystal due to the different stacking modes when they aggregate. Both are distinctly different polymorphs from the same **H** and **G** molecule pair, which

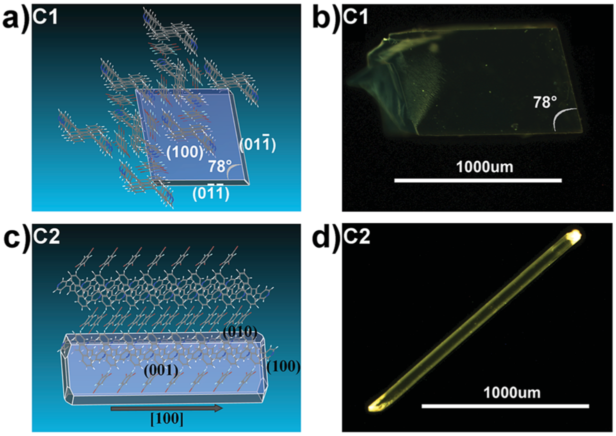

Fig. 3 Predicted growth morphology of (a) C1 and (c) C2. Optical images of (b) C1 and (d) C2 obtained by slow solvent evaporation.

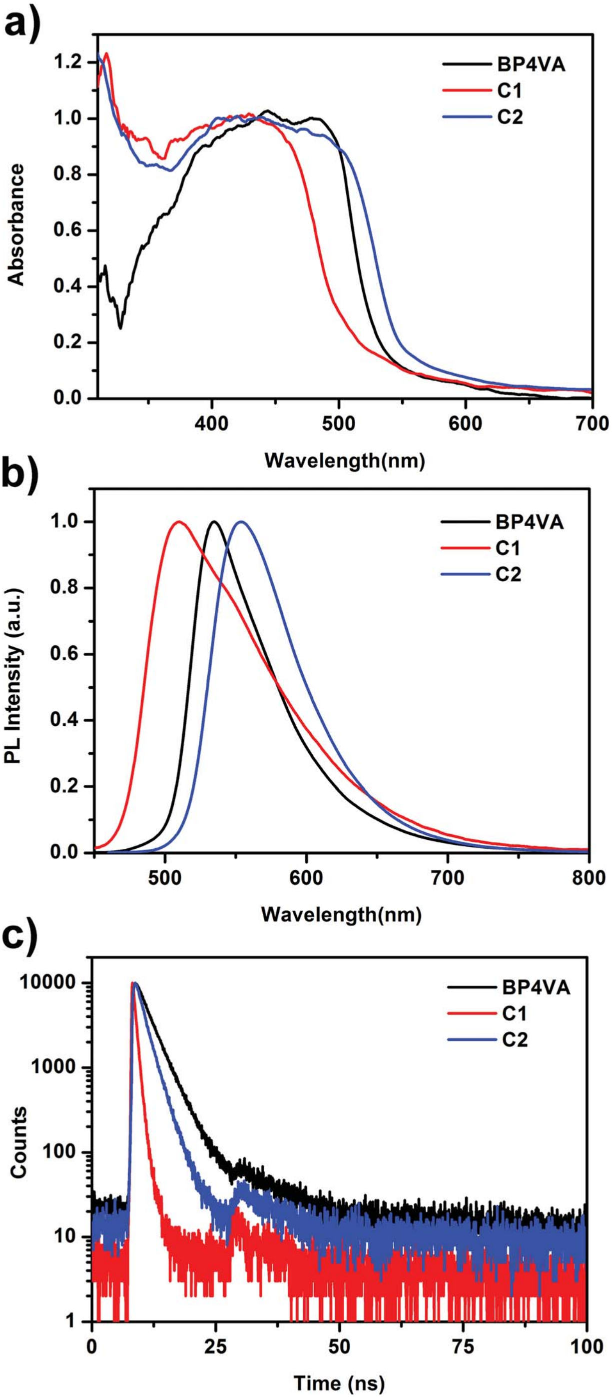

Fig. 4 Absorption spectra (a), PL spectra (b) and time-resolved fluorescence curves (c) of BP4VA and the C1 and C2 crystals, measured on quartz slices.

Table 1 Photophysical properties of BP4VA in THF, and the BP4VA, C1 and C2 crystals[a]

Samples	PL (nm)	Φ_F (%)	$\langle\tau\rangle$ (ns)	k_r (s^{-1})	k_{nr} (s^{-1})
In THF	583	0.365	3.44	1.06×10^8	1.84×10^8
BP4VA	535	0.503	3.62	1.39×10^8	1.37×10^8
C1	510	0.020	1.08	1.85×10^8	9.07×10^8
C2	554	0.342	2.52	1.36×10^8	2.61×10^8

[a] Abbreviations: Φ_F: fluorescence quantum yield determined using a calibrated integrating sphere, average lifetime: $\langle\tau\rangle = (A_1\tau_1{}^2 + A_2\tau_2{}^2)/(A_1\tau_1 + A_2\tau_2)$. Radiative transition rate constant: $k_r = \Phi_F/\langle\tau\rangle$. Non-radiative transition rate constant: $k_{nr} = (1 - \Phi_F)/\langle\tau\rangle$.

will deliver diverse luminescent properties. The significant difference in luminescence between the two polymorphs C1 and C2 is surprising at a first glance, since AIE-active luminogens with a twist conformation mostly show strong emission in the crystalline state.

By the introduction of **G** molecules, the stacking fashion of the chromophore has been changed. For co-crystal C1, there are strong H-type interactions between the **H** and **G** molecules, while for co-crystal C2, the **H** molecules adopt J-aggregation. As we expected, the C2 crystal shows bright yellow emission peaking at 554 nm under UV illumination, with a high quantum yield (Φ_F) of 34%. However, C1 exhibits weak green emission (510 nm) with a very low quantum yield (Φ_F) of 2%. Compared with the pure BP4VA crystal with green emission peaking at 535 nm, C1 shows a 25 nm blue shift, whereas C2 has a 19 nm red shift. It is worth noting that the significance difference in luminescence efficiencies of C1 and C2 is related to the differences in their packing structures. The low Φ_F and blue-shifted fluorescence of C1 can be assigned to the formation of local H-aggregates between **H** and **G** molecules, which often cause nonradiative decay in the highly interacting solid state.[7] This is consistent with the largely blue-shifted absorption band of the C1 crystal compared with that of the pure crystal (Fig. 4). In contrast, there are no obvious π-interactions in the C2 crystal, which allows efficient radiative transition and thus enhanced fluorescence emission. In addition, the C2 crystal

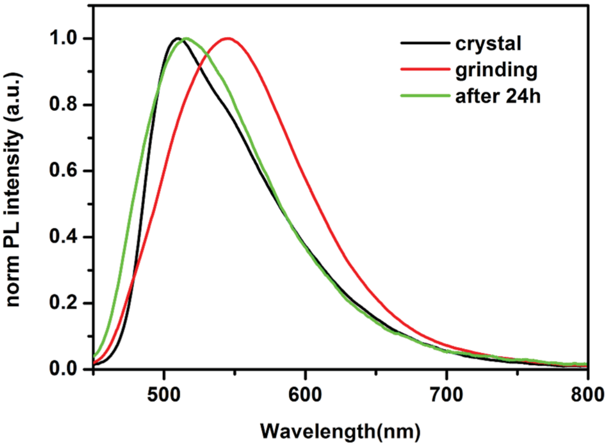

Fig. 5 PL spectra of the initial crystal C1, after grinding and after keeping for 24 h.

displays red-shifted spectra of both absorption and emission compared to those of the pure crystal, which may come from the decreased dihedral angle of the molecule and extended π-conjugation in the crystalline state.

To obtain further insight into the photophysical properties and excited state information of the two polymorphs, the lifetimes (τ_{FL}) of these crystals were measured, and the corresponding emission decay curves are shown in Fig. 4c. The lifetime of co-crystal C1 (1.08 ns) and C2 (2.52 ns) decreased significantly compared to that of the pure crystal (3.62 ns). Because Φ_F is equal to the product of τ_{FL} and the radiative deactivation rate (k_r), k_r and the non-radiative deactivation (k_{nr}) can be approximately estimated as listed in Table 1.

To explore the potential applications of these co-crystals, we investigated the mechanochromic properties of the two co-crystals. Interestingly, the weakly emissive C1 crystal gives more intense emission after being ground. The difference between the emissions of the pristine and the ground crystal is sufficiently large as to be easily distinguished by the naked eye. Moreover, the emission of the ground crystal can recover to the initial state by itself after 24 hours at room temperature. Notably, the emission peak changes from the initial 510 nm to the final 546 nm under grinding, whereas it returns to 515 nm after 24 hours as shown in Fig. 5. There is a small difference in the spectrum between the initial crystal and the recovered crystal, which may originate from the existence of the remaining metastable phase after grinding. This unique mechanochromic behaviour may provide a new way to design and develop novel stimuli-responsive materials.

Conclusions

In summary, two polymorphs of a supramolecular co-crystal (C1 and C2) are prepared by self-assembly with an AEE-active luminogen (BP4VA) as the luminescent host molecule and FIB as the guest molecule. Through manipulating the self-assembly process, various supramolecular interactions such as π–π interactions, halogen or hydrogen bonds, induced the formation of distinct stacking modes. C1 shows weak green emission peaking at 510 nm with a low Φ_F of 2%, due to strong π–π interactions between the **H** and **G** molecules and the formation of local H-aggregates. In contrast, bright yellow emission located at 554 nm with a high Φ_F of 34% was observed from the C2 crystal, since there are no obvious strong intermolecular interactions among the **H** molecules. Furthermore, C1 exhibits a unique mechanochromic behaviour, where its fluorescence shows a red shift after grinding and recovers back to the initial state by itself. These observations demonstrate that manipulating the supramolecular interactions of the co-crystal can not only control the stacking mode but also tune the optical properties. Owing to the diversity and versatility of organic molecular crystals, we expect that the combination of AIE with supramolecular self-assembly will provide a new flexible and controllable strategy for the design of highly efficient supramolecular luminescent systems and the development of novel functions for organic luminescent materials.

Acknowledgements

This work was supported by (2013CB834701), the Natural Science Foundation of China (No. 51373063, 51573068, 21221063) and Program for Chang Jiang

Scholars, Innovative Research Team in University (No. IRT101713018) and Program for Changbaishan Scholars of Jilin Province.

Notes and references

1 R. H. Friend, R. W. Gymer, A. B. Holmes, J. H. Burroughes, R. N. Marks, C. Taliani, D. D. C. Bradley, D. A. Dos Santos, J. L. Brédas, M. Lögdlund and W. R. Salaneck, *Nature*, 1999, **397**, 121.
2 R. Hu, N. L. C. Leung and B. Z. Tang, *Chem. Soc. Rev.*, 2014, **43**, 4494.
3 J. Liang, B. Z. Tang and B. Liu, *Chem. Soc. Rev.*, 2015, **44**, 2798.
4 Q. Chen, H. Fang, B. Xu, J. Yang, H. Xia, F. Chen, W. Tian and H. Sun, *Appl. Phys. Lett.*, 2009, **94**, 201113.
5 S. Varghese and S. Das, *J. Phys. Chem. Lett.*, 2011, **2**, 863.
6 J. Cornil, D. Beljonne, J. P. Calbert and J. L. Brédas, *Adv. Mater.*, 2001, **13**, 1053.
7 F. C. Spano, *Acc. Chem. Res.*, 2010, **43**, 429.
8 J. Luo, Z. Xie, J. W. Y. Lam, L. Cheng, H. Chen, C. Qiu, H. S. Kwok, X. Zhan, Y. Liu, D. Zhu and B. Z. Tang, *Chem. Commun.*, 2001, 1740.
9 Y. Hong, J. W. Y. Lam and B. Z. Tang, *Chem. Soc. Rev.*, 2011, **40**, 5361.
10 Y. Hong, J. W. Y. Lam and B. Z. Tang, *Chem. Commun.*, 2009, 4332.
11 J. Mei, N. L. C. Leung, R. T. K. Kwok, J. W. Y. Lam and B. Z. Tang, *Chem. Rev.*, 2015, **115**, 11718.
12 J. Zhang, B. Xu, J. Chen, S. Ma, Y. Dong, L. Wang, B. Li, L. Ye and W. Tian, *Adv. Mater.*, 2014, **26**, 739.
13 J. Chen, C. C. W. Law, J. W. Y. Lam, Y. Dong, S. M. F. Lo, I. D. Williams, D. Zhu and B. Z. Tang, *Chem. Mater.*, 2003, **15**, 1535.
14 Z. Zhao, J. W. Y. Lam and B. Z. Tang, *J. Mater. Chem.*, 2012, **22**, 23726.
15 D. Ding, K. Li, B. Liu and B. Z. Tang, *Acc. Chem. Res.*, 2013, **46**, 2441.
16 X. Li, K. Ma, S. Zhu, S. Yao, Z. Liu, B. Xu, B. Yang and W. Tian, *Anal. Chem.*, 2014, **86**, 298.
17 K. Ma, H. Wang, H. Li, S. Wang, X. Li, B. Xu and W. Tian, *Sens. Actuators, B*, 2016, **230**, 556.
18 Y. Liu, C. Deng, L. Tang, A. Qin, R. Hu, J. Z. Sun and B. Z. Tang, *J. Am. Chem. Soc.*, 2011, **133**, 660.
19 Z. Wang, B. Xu, L. Zhang, J. Zhang, T. Ma, J. Zhang, X. Fu and W. Tian, *Nanoscale*, 2013, **5**, 2065.
20 L. Yan, Y. Zhang, B. Xu and W. Tian, *Nanoscale*, 2016, **8**, 2471.
21 Y. Zhang, Y. Chen, X. Li, J. Zhang, J. Chen, B. Xu, X. Fu and W. Tian, *Polym. Chem.*, 2014, **5**, 3824.
22 Z. Chi, X. Zhang, B. Xu, X. Zhou, C. Ma, Y. Zhang, S. Liu and J. Xu, *Chem. Soc. Rev.*, 2012, **41**, 3878.
23 Y. Dong, B. Xu, J. Zhang, X. Tian, L. Wang, J. Chen, H. Lv, S. Wen, B. Li, L. Ye, B. Zou and W. Tian, *Angew. Chem., Int. Ed.*, 2012, **51**, 10782.
24 J. Zhang, J. Chen, B. Xu, L. Wang, S. Ma, Y. Dong, B. Li, L. Ye and W. Tian, *Chem. Commum.*, 2013, **49**, 3878.
25 J. Chen, S. Ma, J. Zhang, L. Wang, L. Ye, B. Li, B. Xu and W. Tian, *J. Phys. Chem. Lett.*, 2014, **5**, 2781.
26 Q. Qi, J. Qian, X. Tan, J. Zhang, L. Wang, B. Xu, B. Zou and W. Tian, *Adv. Funct. Mater.*, 2015, **25**, 4005.
27 S. I. Stupp and L. C. Palmer, *Chem. Mater.*, 2014, **26**, 507.

28 W. Zhu, R. Zheng, X. Fu, H. Fu, Q. Shi, Y. Zhen, H. Dong and W. Hu, *Angew. Chem., Int. Ed.*, 2015, **54**, 6785.

29 W. Zhu, R. Zheng, Y. Zhen, Z. Yu, H. Dong, H. Fu, Q. Shi and W. Hu, *J. Am. Chem. Soc.*, 2015, **137**, 11038.

30 S. K. Park, S. Varghese, J. H. Kim, S. Yoon, O. K. Kwon, B. An, J. Gierschner and S. Y. Park, *J. Am. Chem. Soc.*, 2013, **135**, 4757.

31 Y. Dong, J. Zhang, X. Tan, L. Wang, J. Chen, B. Li, L. Ye, B. Xu, B. Zou and W. Tian, *J. Mater. Chem. C*, 2013, **1**, 7554.

32 V. Bernard, *Molecular Fluorescence Principles and Applications*, Wiley-VCH, Weinheim, Germany, 2002.

33 C. A. Hunter and J. K. M. Sanders, *J. Am. Chem. Soc.*, 1990, **112**, 5525.

34 Y. Umezawa, S. Tsuboyama, K. Honda, J. Uzawa and M. Nishio, *Bull. Chem. Soc. Jpn.*, 1998, **71**, 1207.

35 S. Tsuzuki, *Annu. Rep. Prog. Chem., Sect. C: Phys. Chem.*, 2012, **108**, 69.